Modeling near-field effects in VSP-based Q-estimation

Arnim B. Haase and Robert R. Stewart

ABSTRACT

The complete spherical wavefield emanating from a P-wave point source surrounded by a homogeneous isotropic medium is computed with the aid of Sommerfeld/Weyl integrals. In a resulting synthetic VSP, we observe a near-field, a far-field and a 90° phase rotation between the two. Depth dependence of magnitude spectra in these two depth regions is distinctly different. Log magnitude spectra show a linear dependence on frequency in the far-field but not in depth regions where the near-field becomes significant. Near-field effects are one possible explanation for large positive and even negative Q-factors in the shallow section that may be estimated from VSP data when applying the spectral ratio method.

INTRODUCTION

Why is attenuation (Q) estimation still a research topic after all these years of investigation? Seismic quality factors Q are sought because Q-compensation increases resolution and Q could serve as a seismic attribute describing rock properties. What, then, are the practical difficulties encountered in attenuation (Q) estimation? According to Best (2007) there are three main reasons for our struggle:

1) restricted bandwidth,

2) poorly constrained multiple scattering, and

3) geometric spreading losses.

By contrast, the popular spectral ratio method of Q-estimation is derived for plane-waves propagating in a homogeneous medium. The seismic wavefield is composed of near-field as well as far-field contributions. We expect plane-wave theory to break down in the near-field, but what is the extent of this region and what is the size of Q-estimation errors there? It has been observed that VSP-based Q-estimates can give negative values for the near surface. For example, Raikes and White (1984) noted negative Q and attributed their result to a change in geophone coupling. This possibility is included in our own list (Haase and Stewart, 2006a) which comprises

1) acquisition issues,

2) analysis problems and

3) lithology-model inadequacies.

In pursuing the topic of stratigraphic attenuation, we recently computed synthetic VSP data with the aid of Weyl/Sommerfeld integrals (Haase and Stewart, 2007) and noted some peculiar behaviour of magnitude spectra as a function of depth in near-

surface situations. The cause for this strange departure from far-field expectations turns out to be, not surprisingly, a near-field contribution to the total wave field of a P-wave point source.

Also interesting is the behaviour of near-field magnitude spectra as a function of frequency. Kjartansson (1979) mentions that Q is mildly frequency dependent but then proceeds with a constant Q assumption. Frequency dependent near surface Q-factors have also been observed in the Alberta oil sands (K. Hedlin, 2007, personal communication).

The aim of this study is to show that near-field behaviour is another possible explanation for negative Q-estimates and frequency-dependent Q in the near-surface.

THEORY

From a wide variety of Q-estimation techniques developed over the years, the spectral ratio method (SRM) appears to be the most commonly used approach. The derivation of Q-estimation methods is usually based on the definition of the quality factor Q. For the spectral ratio method Tonn (1991) gives

$$\ln\left[\frac{A_1(\omega)}{A_0(\omega)}\right] = -\frac{\omega t}{2Q}, \qquad (1)$$

where the geometric spreading ratio is ignored and Q >> 1 is assumed.

In case of a homogeneous medium, Q-factors can be recovered exactly (within numerical accuracy) under far-field conditions when the source-receiver separation is large. What are these far-field conditions and when do they break down? Aki and Richards (1980) use the phrase "*many wave lengths*" when describing the far-field distance from a point source. They give an equation for the P-wave potential caused by a point source (Weyl/Sommerfeld integral approach) in a 3D homogeneous medium. P-wave displacements can be obtained from such potentials by computing gradients, which for the direct wave gives (Haase and Stewart, 2007)

$$u_P(\omega) = i\omega e^{-i\omega t}\int_0^\infty \left[\frac{p^2}{\xi}J_1(\omega pr)\sin(\theta) - ipJ_0(\omega pr)\cos(\theta)\right]e^{i\omega z\xi}dp, \qquad (2)$$

where $u_P(\omega)$ is the P-wave displacement along the ray at the current receiver and ω,

ω is the frequency in radians,

t is the time,

p is the horizontal slowness,

ξ is the vertical slowness,

J_0 and J_1 are zero-order and first-order Bessel functions of the first kind,

r is the range (horizontal offset between source and receivers),

z is the source-to-receiver depth interval (to the current receiver) and

θ is the incidence angle from the vertical (at the current receiver).

The P-wave displacements along the ray, computed with Equation 2, are obtained by integration over (always) real horizontal slowness p, one frequency point at a time. Because of finite Q-factors all velocities are complex; also the vertical slowness ξ is complex, even outside the evanescent region. The Bessel functions in Equation 2 are the result of, firstly, integrating over azimuth when deriving the Sommerfeld-integral from the Weyl-integral (describing the 3D nature of the problem by J_0) and, secondly, taking the gradient of potentials to obtain displacements (adding a J_1-term). The last term in Equation 2, that is $e^{i\omega z\xi}$, represents a travel-time term. As we will see below, displacements computed with Equation 2 are composed of near-field and far-field contributions. Plane-wave approximations are accurate only in the far-field, as suggested in Figure 1. Close to a source we encounter the near-field term and spherical spreading as well as distance dependent phase changes because of a near-field to far-field change over; we also note that apparent velocities change with depth in the non-zero offset situation of Figure 1.

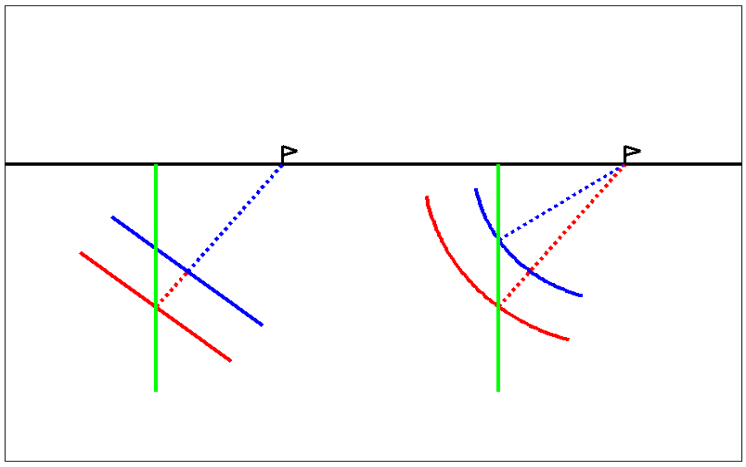

FIG. 1. Elastic plane wave amplitudes are independent of travel distance whereas spherical wave amplitudes encounter spherical spreading.

For the zero-offset (zo) VSP, the range r in both Bessel function arguments is zero. With $J_0(0) = 1$, $J_1(0) = 0$ and introducing $[p\,dp] = [-\xi\,d\xi]$ (obtained from $\xi^2 = 1/V_p^2 - p^2$ and $d\xi/dp = -p/\xi$, where V_p is P-wave velocity), we find

$$u_{P-zo}(\omega) = -\omega e^{-i\omega t} \int_{1/\alpha}^{i\infty} \xi e^{i\omega z\xi} d\xi \quad , \tag{3}$$

which can be integrated analytically giving

$$u\big|_{r=0} = \frac{i\omega}{V_p} e^{-i\omega t}\left[\frac{1}{z} + \frac{iV_p}{\omega z^2}\right] e^{i\omega z/V_p} = \frac{i\omega}{zV_p} e^{-i\omega t}\left[1 + \frac{iV_p}{\omega z}\right] e^{i\omega z/V_p}. \quad (4)$$

The first term in the brackets of Equation 4 is the familiar far-field term. It decays with *1/z*. The second term in brackets decays with $1/z^2$. Because of this more rapid decay, it is noticeable only in the near-field where it can dominate the far-field term at low frequencies thereby mimic a frequency dependent Q. For $\infty > Q >> 1$, there is an almost 90° phase difference between these two terms which should allow separation at least in this homogeneous modeling situation. Note that P-wave velocity V_p is complex for finite Q.

There is another less obvious approximation hidden in the derivation of Equation 1. From the definition of Q (Aki and Richards, 1980), we have

$$A(t) = A_0(1 - \pi / Q)^n \quad (5)$$

which Aki and Richards (1980, page 168) replace by

$$A(t) = A_0 e^{-n\pi/Q} \quad (6)$$

for large *n* (i.e., for large times because $t = 2n\pi/\omega$). However, the resulting Q-estimation error is independent of *n* and increases with decreasing Q-factors. At Q = 100 the departure between actual and estimated Q is only a fraction of a percent which increases to approximately 6% at Q = 10.

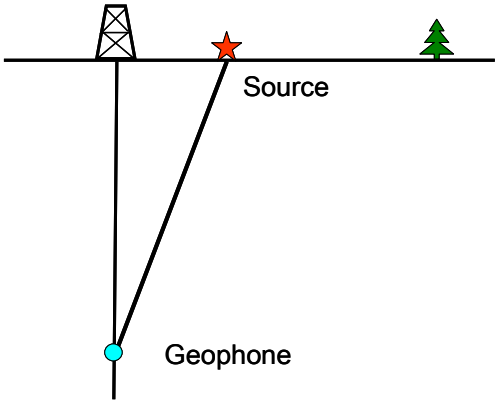

FIG. 2. Zero-offset VSP geometry (assuming that source-offset *x* is much less than geophone depth *z* or *x/z* << *1*).

MODELLING RESULTS

Figure 2 shows the geometry of a vertical seismic profile (VSP). The term "*vertical*" is not to be taken literally for our model-geometry as there usually is non-zero source-to-borehole offset. VSP-receivers, which nowadays tend to be 3-component geophones, are placed in the borehole with a constant depth interval between them. In a real-world VSP these depth stations receive upgoing and downgoing wave fields. In our chosen homogeneous model environment there are no reflections but only the transmitted source wavelet. That is to say our model includes neither surface effects nor geophone clamping

problems nor multiples nor soil compaction. Zero-offset synthetic VSP traces computed with Equation 2 for a homogeneous situation are displayed in Figure 3 (Haase and Stewart, 2007). The parameters for this earth model are

V_p = 2000m/s,

V_s = 879.88m/s,

ρ = 2400kg/m^3 and

Q_p = 100.

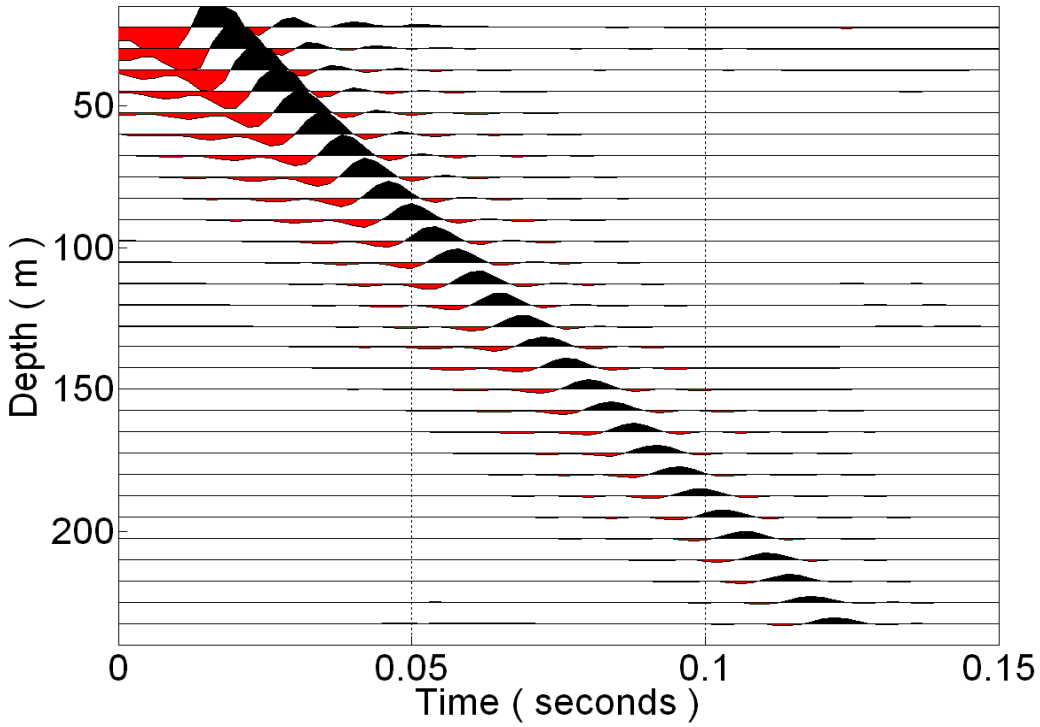

FIG. 3. Zero-offset synthetic VSP computed with Equation 2 for a zero-phase (non-causal) 5/15-80\100Hz Ormsby wavelet.

The zero-phase (non-causal) Ormsby wavelet employed for these computations has the parameters 5/15-80\100 Hz. Amplitude decay with increasing depth is clearly visible. Also note the phase rotation between shallower and deeper traces where deep traces are roughly zero-phase but shallow traces are ~90° phase rotated. As the near-field decays with $1/z^2$ (in contrast to $1/z$ for the far-field) its influence quickly disappears with increasing depth. At shallow depths, where the near-field predominates, we can expect time-domain Q-estimation methods to underestimate Q (overestimate attenuation) because of the $1/z^2$ amplitude decay. Figure 4 gives Q-estimates computed with the analytical signal method (ASM) from the model traces shown in Figure 3.

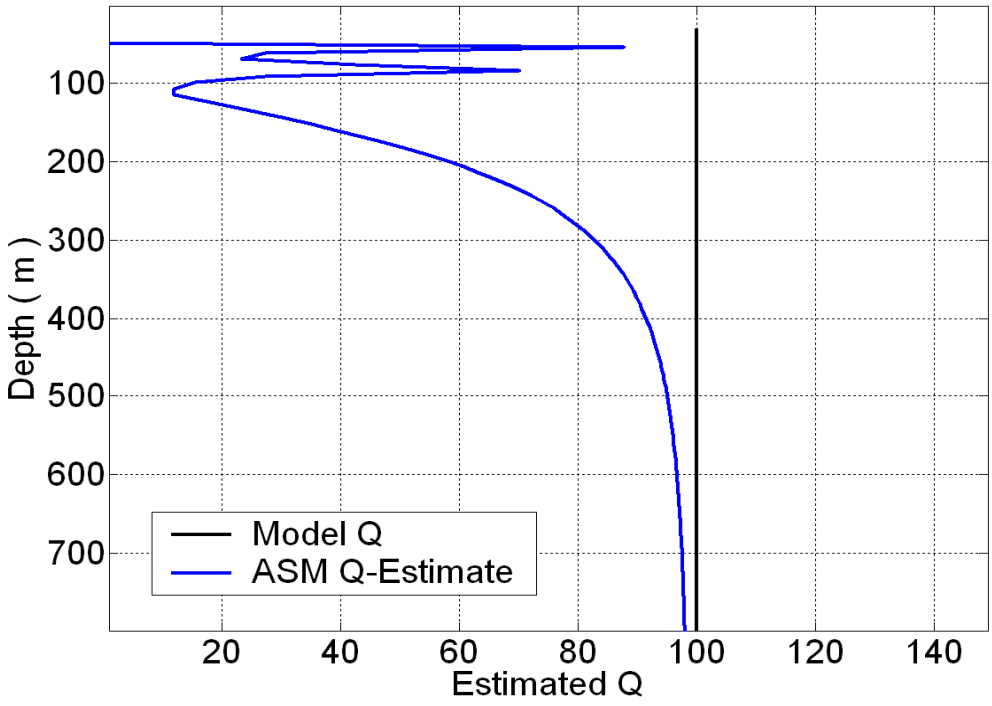

FIG. 4. Analytical signal method Q-estimate computed from the synthetic VSP traces shown in Figure 3 compared to the original model-Q of 100.

ASM is one of the time domain methods of Q-estimation mentioned by Tonn (1991); attenuation is determined from the decay of instantaneous amplitudes. As expected, Q is underestimated in the near-field because of a more rapid amplitude decay proportional to $1/z^2$ being forced upon a $1/z$-estimator. The model Q-factor of 100 is approached at larger depths.

What would be the near-field Q-estimation error for frequency domain estimation techniques? To answer this question we examine near-field and far-field magnitude spectra next. Plotted in Figure 5 are log-magnitude spectra, computed with the Sommerfeld-integral given in Equation 2, for the depth range of 15 m to 61 m. This is thought to be the depth range where the near-field term (decaying with $1/z^2$) dominates the far-field term (decaying with $1/z$). Global scaling to a maximum of zero dB is applied to the spectra in Figure 5; the relative amplitudes are retained. We note that attenuation increases with depth z and frequency ω. Nonlinear frequency dependence of log-magnitude spectra in this depth region could be interpreted as a frequency dependent quality factor Q(ω), however the model computation uses constant Q. Relative scaling is lost when applying the spectral ratio method (SRM) because multipliers become added constants on taking the logarithm; these added constants are part of the neglected intercept term. Figure 6 demonstrates what SRM "sees" (Haase and Stewart, 2007). The downgoing wave "*appears*" to gain high frequency strength: the shallower in depth the VSP-receiver station the steeper the slope of log-magnitude spectra as function of frequency, which implies negative Q-factors. Note that neither geophone coupling nor surface soil compaction are modeled here.

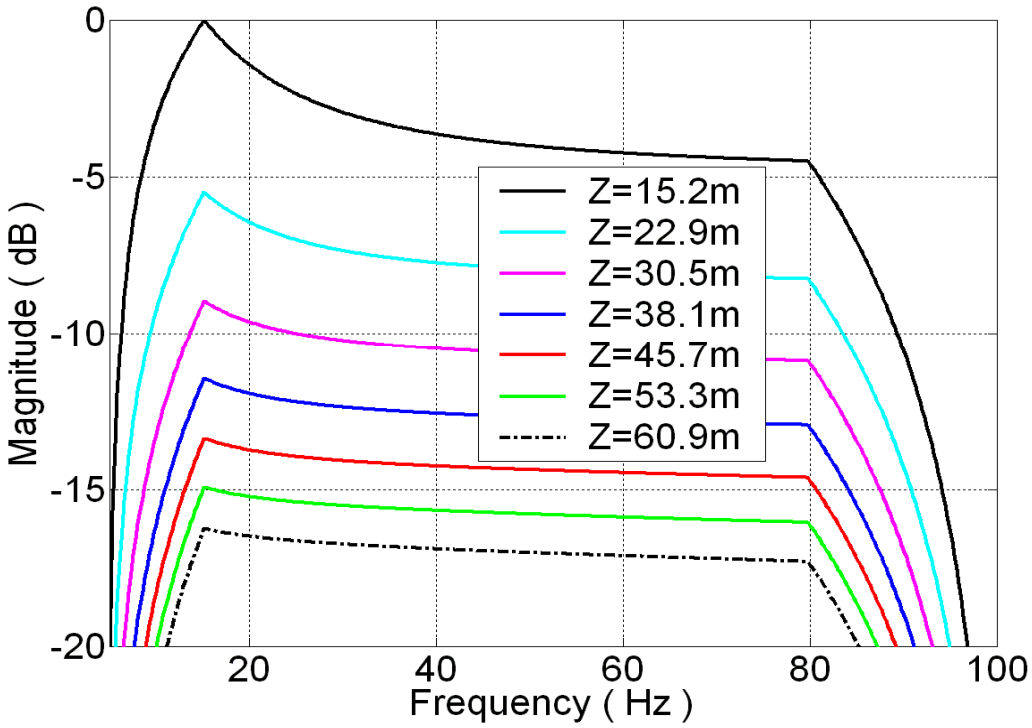

FIG. 5. Near-field log-magnitude spectra for the depth range from 15 m to 61 m computed with the Sommerfeld-integral of Equation 2 (global scaling to zero dB with relative amplitudes retained).

When computing log-spectral ratios between depth levels 15 m and 38 m, we find a curve (Figure 7) which clearly is *not* a linear function of frequency. Fitting straight lines in three different frequency ranges leads to three different (negative) Q-estimates. The frequency range from 55 Hz to 80 Hz appears practically linear in Figure 7 but the enlarged view in Figure 8 displays the influence of plotting scale. It was noted above that log-magnitude spectra plotted in Figure 6 have increased slope angles with decreased depth. Close inspection of the deepest receiver (at 60.9 m depth) above approximately 50 Hz shows a trend change because far-field conditions are approached. Q-estimation leads to negative Q-factors near the source and large positive Q some distance away in the near-field where the slope trend is reversed but the log-magnitude curves are still almost parallel. As far-field conditions are approached the estimated Q converges with the model Q of 100. Q versus depth estimated in two different frequency bands is depicted in Figure 9. Note the "*wrap-around*" look at the depths where Q changes polarity. A real-data heavy oil sand SRM Q-estimation example (Ortiz-Osornio and Schmitt, 2008) can be seen in Figure 10; zero Q is located in the centre of both diagrams. This example for an inhomogeneous "*real world*" appears full of "*wrap-around*" only some of which is eliminated by their method.

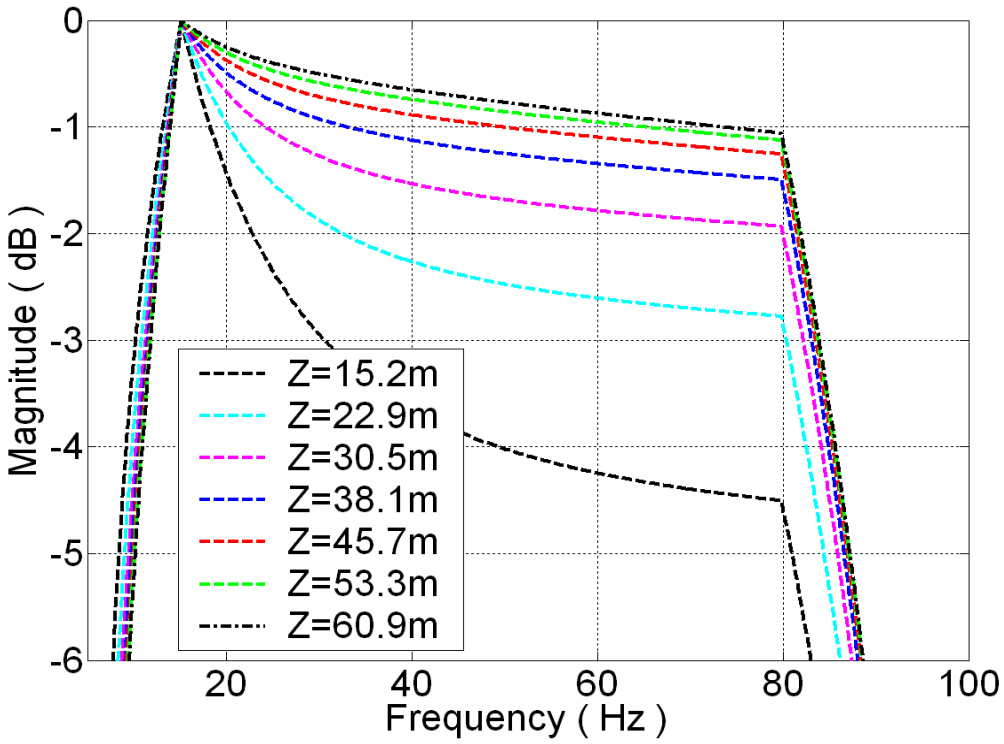

FIG. 6. Near-field log-magnitude spectra with all spectra equalized to their maximum amplitudes (zero dB scaling applied individually. The down going wave *appears* to gain high frequency strength. Note the vertical scale differs from Figure 5.

The frequency dependence of "*wrap-around*" depths visible in Figure 9 is further explored in Figure 11. The smaller the Q-estimation bandwidth and the smaller the centre frequency of this estimation band the larger are "*wrap-around*" depths where *Q(z)* polarity changes are observed. As we increase exploration bandwidth towards lower frequencies we extend near-field effects to larger depths. Figure 12 (Haase and Stewart, 2007) gives log-magnitude spectra for the depth region of 61 m to 1113 m which is below that displayed in Figure 6, again computed with Equation 2. This is the far-field dominated depth region where Q-factor recovery is expected to be almost perfect because spectral ratio methods are derived for these circumstances with linear log ratio slopes. The deeper the receiver, the steeper the log-magnitude curve. All spectra in Figures 6 and 12 are normalized to the same zero dB maximum, but the plotting scales differ between the Figures. Figure 13 compares SRM-derived *Q(z)* to the model Q of 100. We observe ringing in the near-field to far-field transition region and faster convergence to the model Q than the ASM-derived *Q(z)* shown in Figure 4. Note that negative Q-factors are not plotted in this diagram. This kind of "*near-field behaviour"* has also been observed by the authors when estimating Q from actual VSP data. A real data example (Haase and Stewart, 2006b) is shown in Figure 14. This example is from southern Saskatchewan, Canada, where no permafrost exists and high near-surface Q-factors are unexpected (and unrealistic). In fact, most of the authors' VSP-data examples show this near-surface trend.

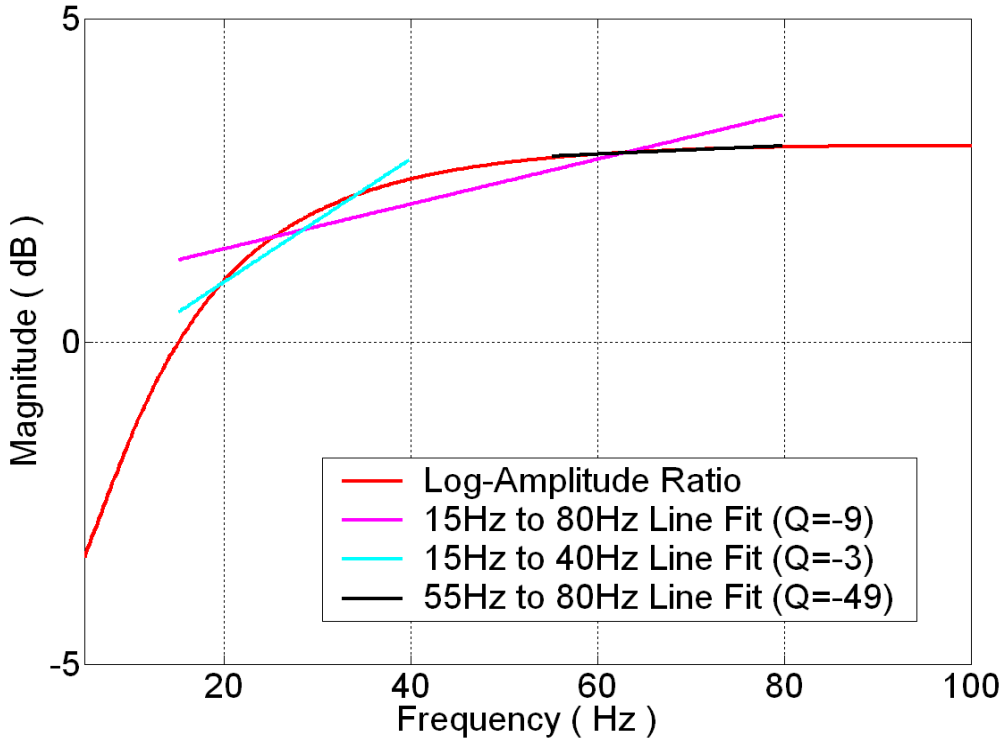

FIG. 7. Straight line fit to the log spectral ratio between depth levels 15m and 38m.

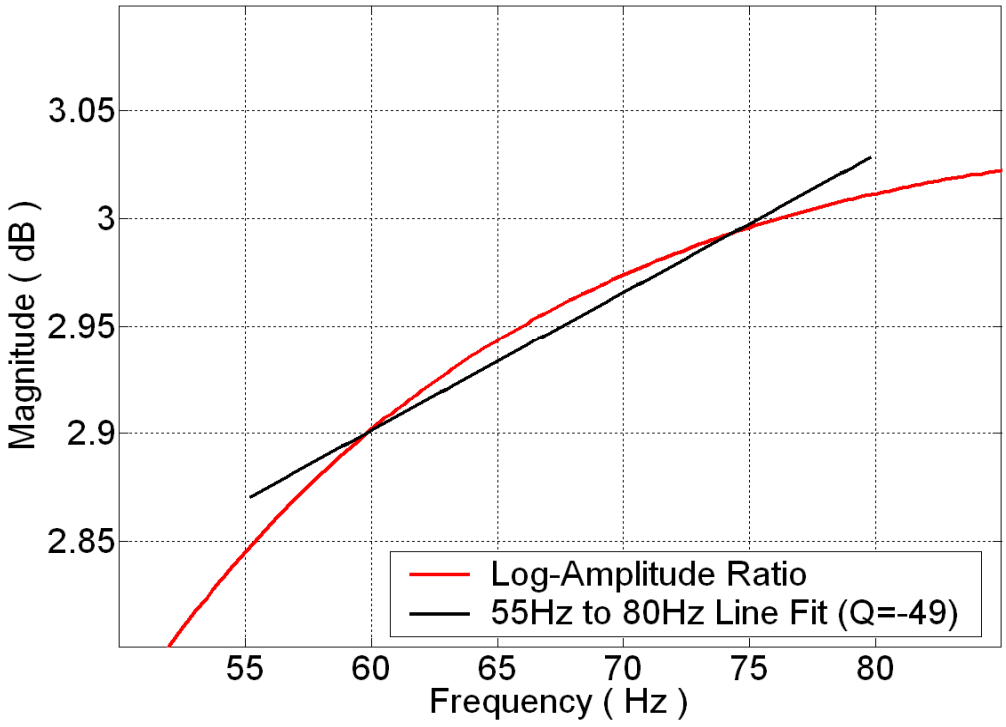

FIG. 8. Enlarged view of Figure 7. Any straight-line appearance of log-ratios depends on scale.

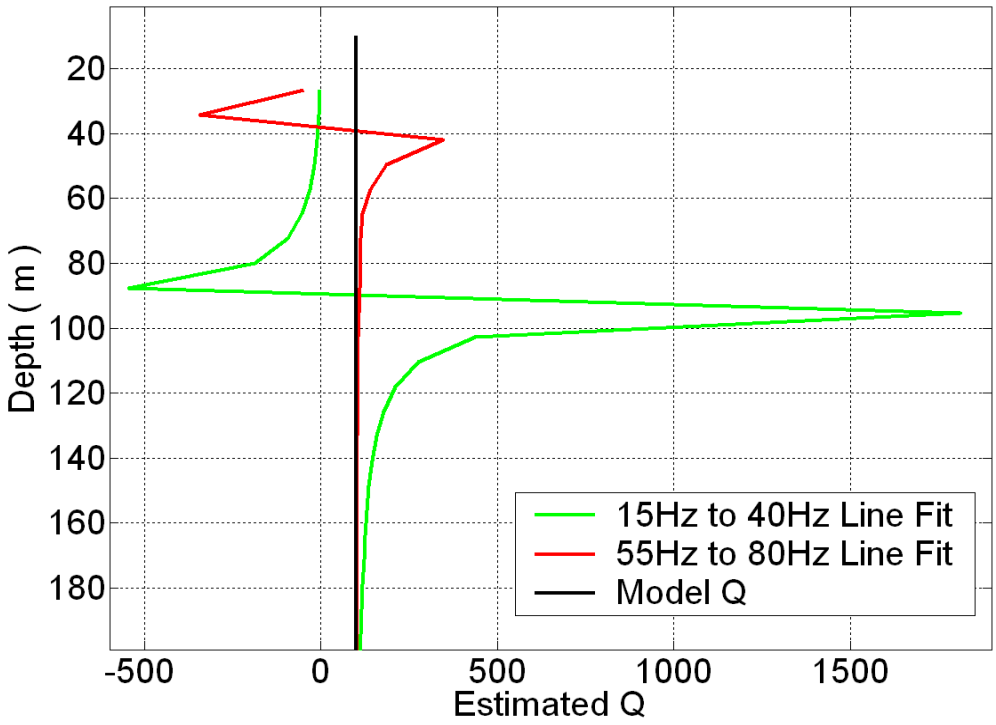

FIG. 9. Apparent near-field frequency dependence of Q. Note the polarity change of Q.

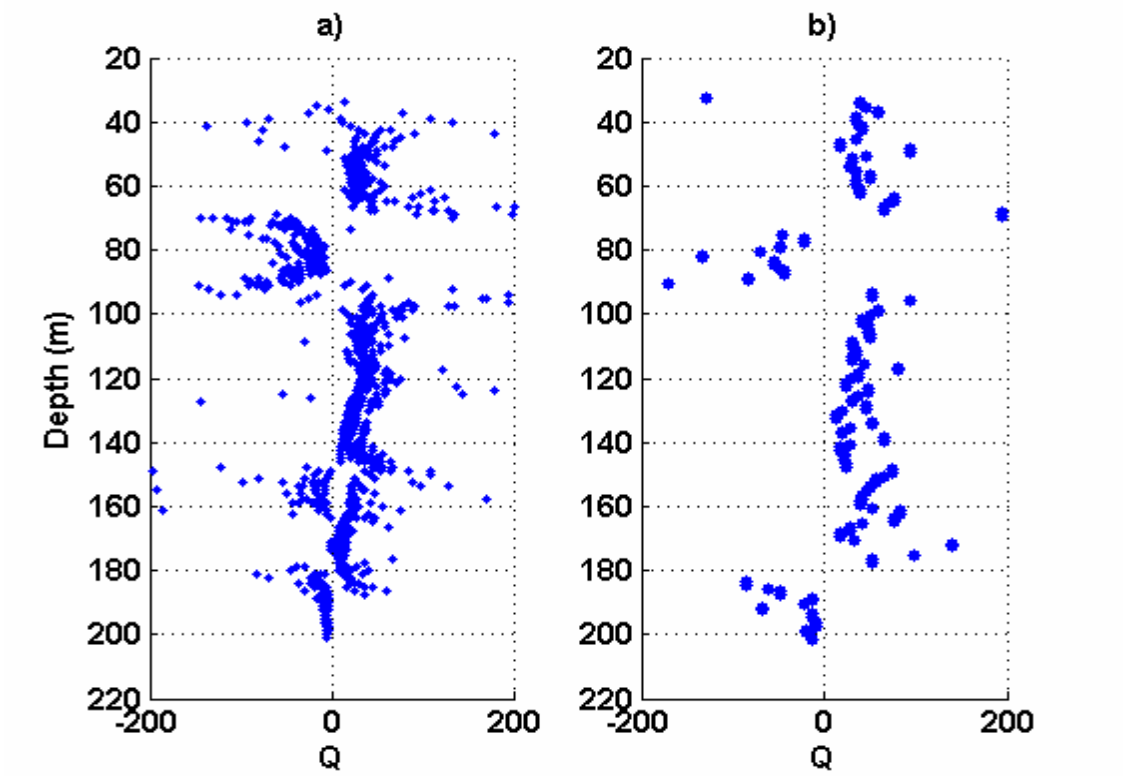

FIG. 10. Heavy oil sand Q-factors [Ortiz-Osornio and Schmitt, 2008: a) the traditional spectral ratio technique, and b) the inversion algorithm].

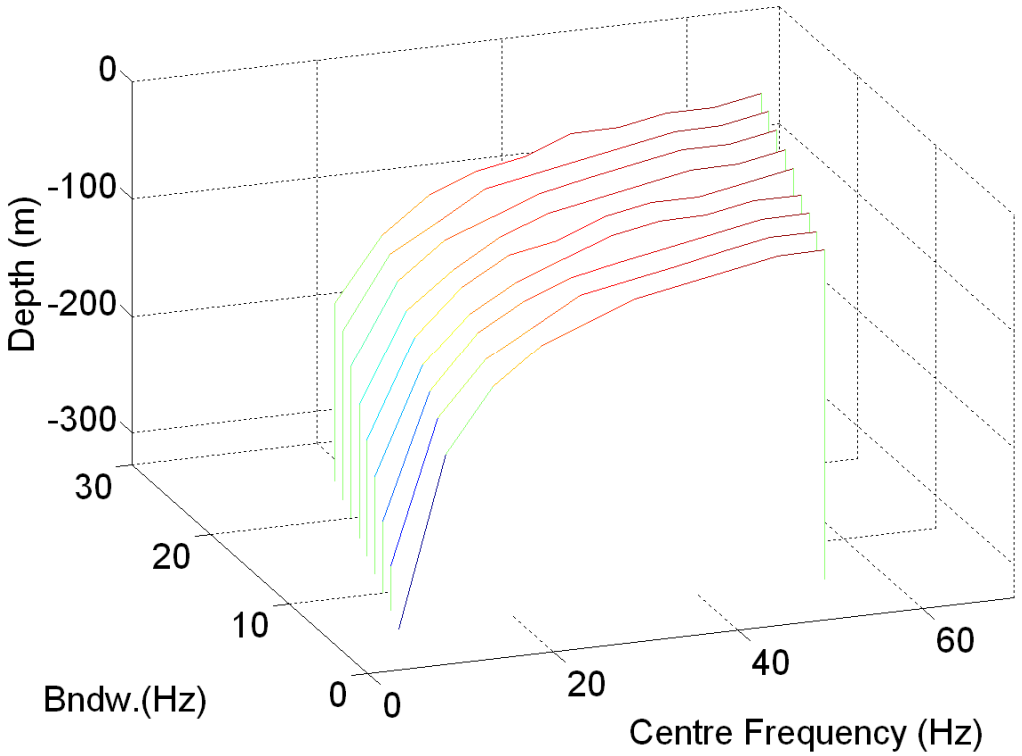

FIG. 11. Depth of Q-polarity change as function of centre-frequency and bandwidth.

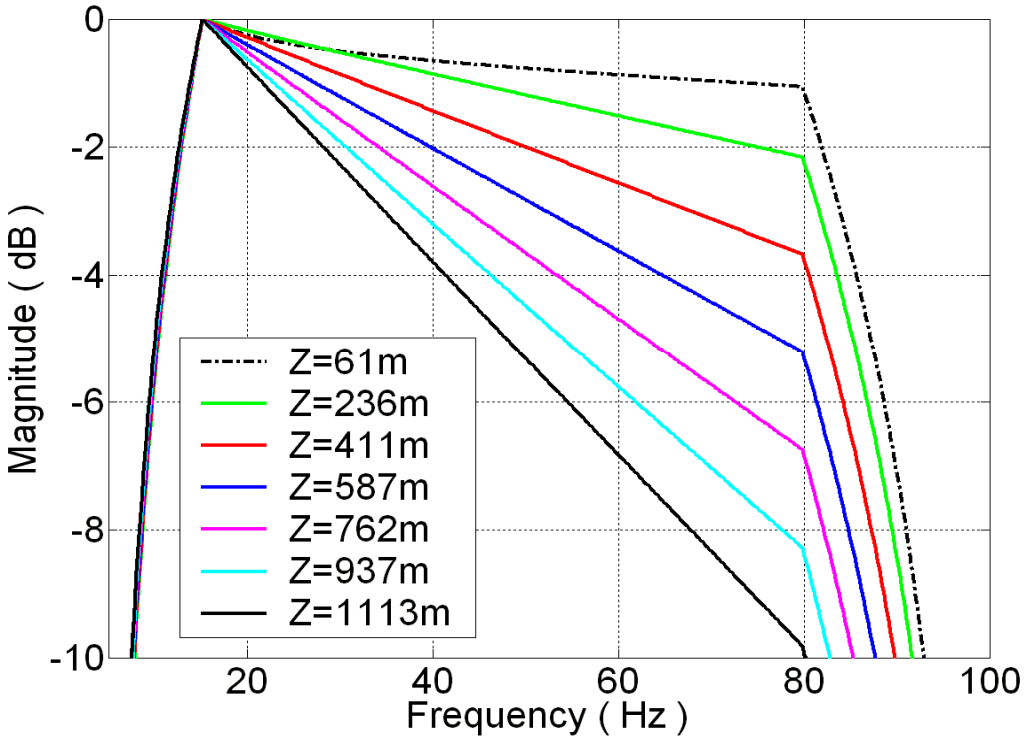

FIG. 12. Far-field log-magnitude spectra with zero dB scaling applied individually.

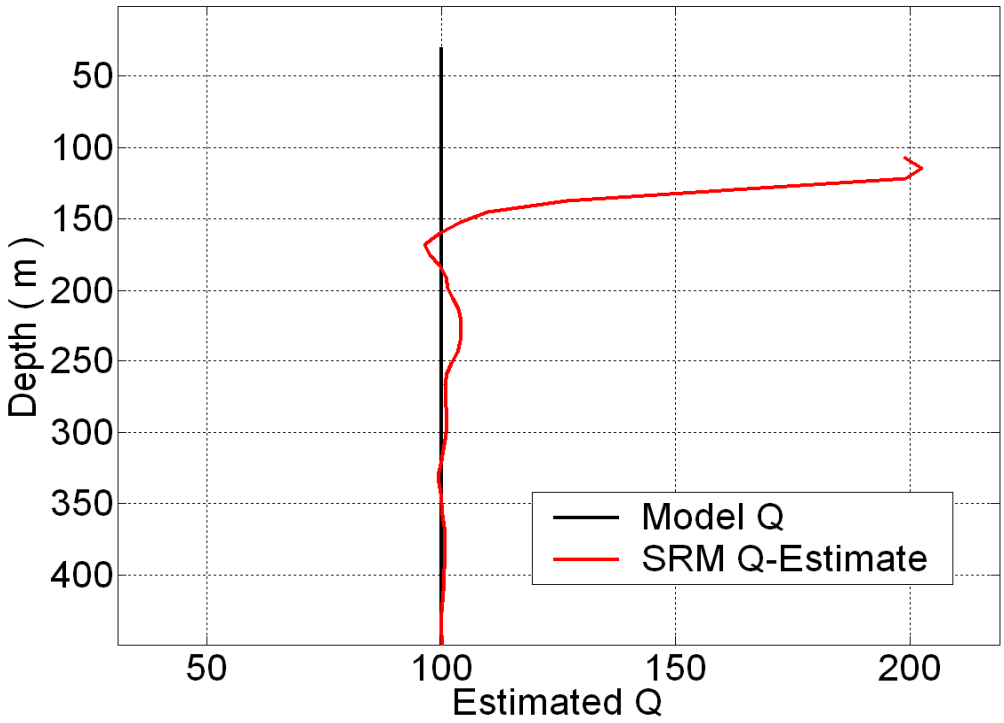

FIG. 13. Spectral ratio method Q-estimate computed from the synthetic VSP traces shown in Figure 3 compared to the original model-Q of 100.

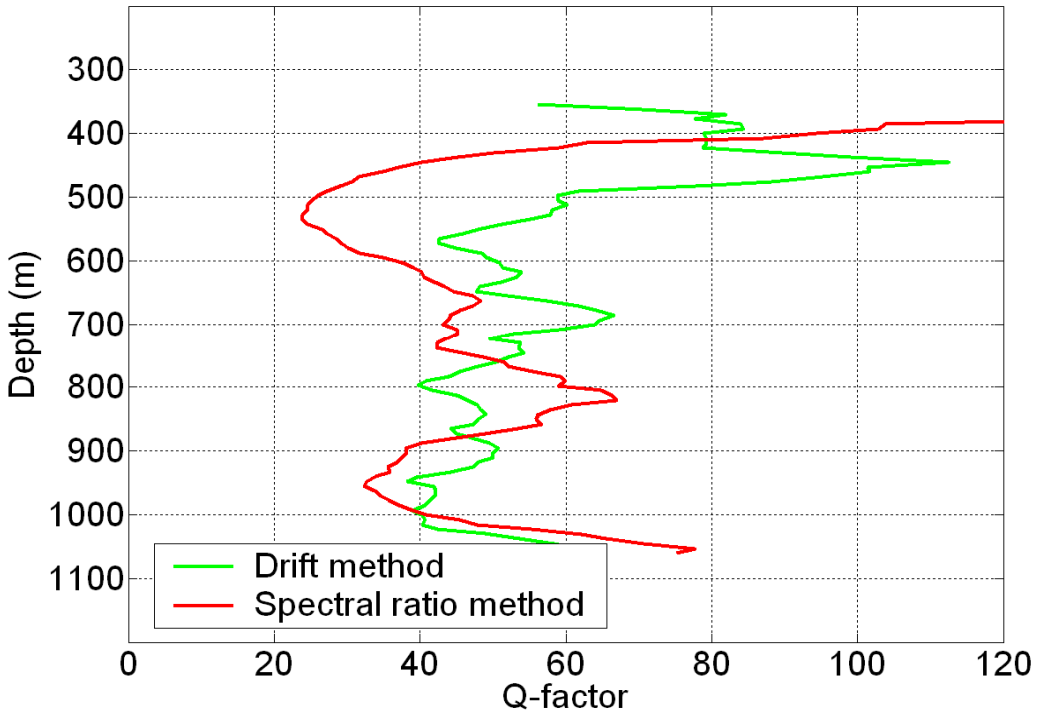

FIG. 14. Q versus depth for zero-offset VSP data acquired at Ross Lake, Saskatchewan.

Where does the near-field stop and the far-field begin? Aki and Richards (1980) use the term "*many wavelengths*" when describing the distance from source points to where far-field approximations start to be accurate. Common practice is to assume that "*several wavelengths*" are sufficient for far-field approximation accuracy (E. Krebes, 2007, personal communication). From Equation 4, it is clear that near-fields diminish with increasing depth z and increasing frequency ω relative to the far-field. The term $\alpha/(\omega z)$ in Equation 4 is proportional to λ/z where λ is the wave length. In Figure 15, λ/z is plotted as a function of z and ω. The maximum value of 1.0 represents the case of $\lambda=z$ and the minimum of 0.1 stands for $z=10\lambda$. At 10 Hz, the 10% threshold is as deep as z=2000 m; in the other extreme at z=200 m the frequency must be increased to 100 Hz in order to reach the same 10% threshold. If we take the "*many wavelengths*" to mean 10λ then this prescribes a minimum evaluation frequency of 40 Hz for a depth of 500 m. "*Near-field*" and "*near-surface*" may not be strictly interchangeable. In reality, a 10λ cut-off is probably too restrictive because of the phase difference between near-field and far-field.

NEAR-FIELD COMPENSATION OF Q-ESTIMATION

From Equation 4 it is clear that all amplitudes are multiplied by a factor of $(1+iV_p/\omega z)$. In the far-field where depth z is large, and/or at higher frequencies ω, this multiplier approaches unity. As a first step we try to precondition the input spectra prior to Q-estimation through division by this factor. Because the spectral ratio method operates on amplitudes, and ignores phase information, we proceed with the magnitude of this multiplier. Spectra thus compensated are plotted in Figure16. When comparing to Figure 6 we note that, firstly, the near-field compensated spectra are much less curved and, secondly, their slopes increase with depth. The second point constitutes a complete reversal of the near-field *behaviour* observed in Figure 6. The steady increase of compensated spectral slopes with depth now precludes negative Q-factors. However, close inspection of Figure 16 reveals that spectral slopes "*move"* further apart with decreasing depths. This slope diversion and also any remnant curvature are expected to cause Q-estimation errors. Figure 17 shows that simply near-field compensating amplitude spectra does improve Q-estimates to a certain extent. There are no negative Q-values in the new Q-estimate but at very shallow depths (above approximately 100 m) the quality factor is grossly underestimated.

CONCLUSIONS

The near-field of a P-wave point source decays faster with distance from the source than the far-field ($1/z^2$ versus $1/z$). It also decays with frequency. The combined near-field factor is $V_p/(\omega z)=\lambda/(2\pi z)$ and for $V_p/(\omega z)<<1$ far-field conditions apply. Because of the more rapid decay of low frequencies close to the source there is a "*relative*" increase in strength of high frequencies in this region leading to negative Q-estimates when the spectral ratio method is applied here. At some distance from the source, where log magnitude curves are parallel, the estimated Q would be infinite. Just beyond that (further away from the source point) Q-estimates show large positive values which will decrease towards the model-Q as the source-to-receiver distance is further increased and far-field conditions are approached.

There is also a bias error in SRM Q-estimates that depends on 1/Q only and not on source-to-receiver separation. For Q=100 this error is only a fraction of a percent; it increases to approximately 6% for Q=10.

ACKNOWLEDGEMENTS

The authors wish to thank Dr. C. Ursenbach for helpful discussions related to the mathematical development. Support from the CREWES Project at the University of Calgary and its industrial sponsorship is gratefully acknowledged.

REFERENCES

Aki, K.T., and Richards, P.G., 1980, Quantitative Seismology: Theory and Methods: Vol. 1, W.H. Freeman and Co.

Best, A.I., 2007, Introduction to Special section – Seismic Quality Factor: Geophysical Prospecting, **55**, 607-608.

Haase, A.B., and Stewart, R.R., 2006a, Stratigraphic attenuation of seismic waves: CREWES Research Report, **18**.

Haase, A.B., and Stewart, R.R., 2006b, Estimating Q from VSP data: Comparing spectral ratio and analytical signal methods: CREWES Research Report, **18**.

Haase, A.B., and Stewart, R.R., 2007, Testing VSP-based Q-estimation with spherical wave models: CREWES Research Report, **19**.

Kjartansson, E., 1979, Constant Q, wave propagation and attenuation: Journal of Geophysical Research, **84**, 4737-4748.

Ortiz-Osornio, M., and Schmitt, D., 2008, Q Inversion in a Heavy Oil Sand: Annual CSEG Meeting (2008 C3GEO Convention), Expanded Abstracts, 489-492.

Raikes, S.A., and White, R.E., 1984, Measurements of earth attenuation from downhole and surface seismic recordings: Geophysical Prospecting, **32**, 892-919.

Tonn, R., 1991, The determination of seismic quality factor Q from VSP data: A comparison of different computational methods: Geophysical Prospecting, **39**, 1-27.

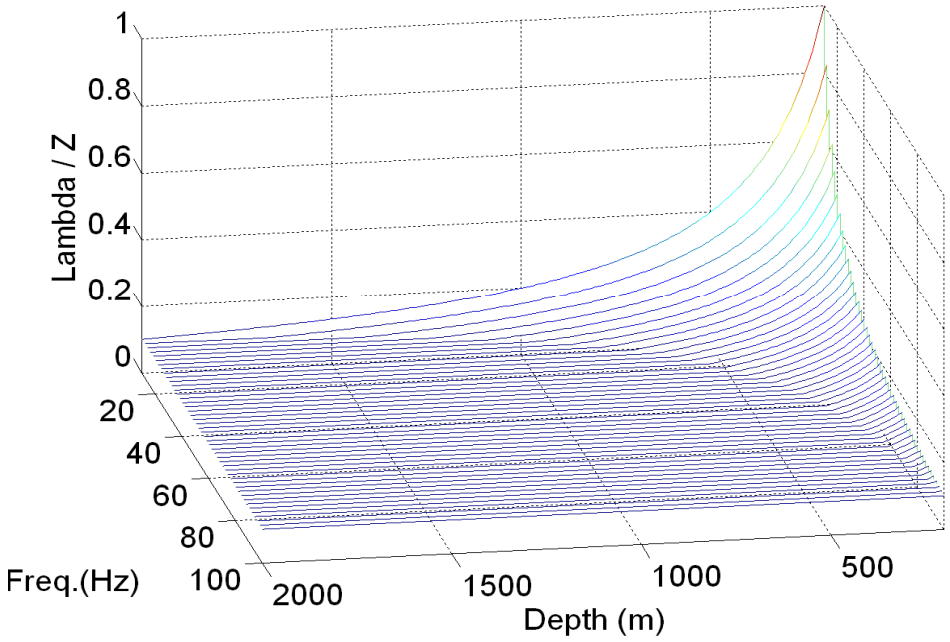

FIG. 15. Relative near-field strength (λ/z) plotted as function of depth z and frequency ω/(2π). Note the 10% cutoff.

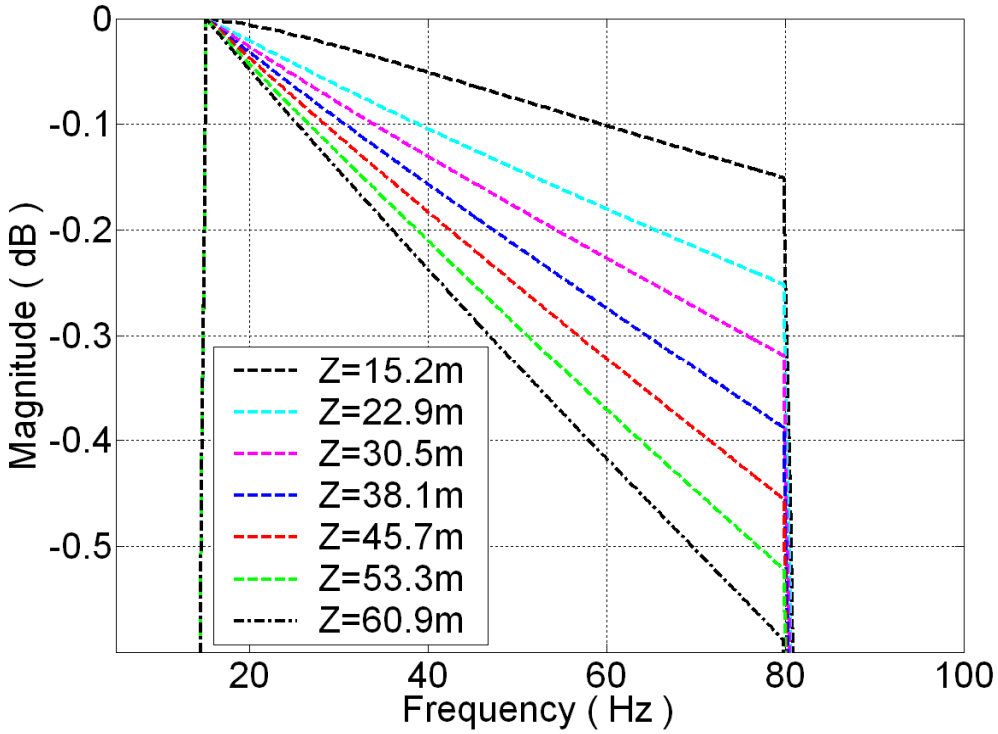

FIG. 16. Near-field log-magnitude spectra with near-field compensation applied (compare to Figure 6 without compensation).

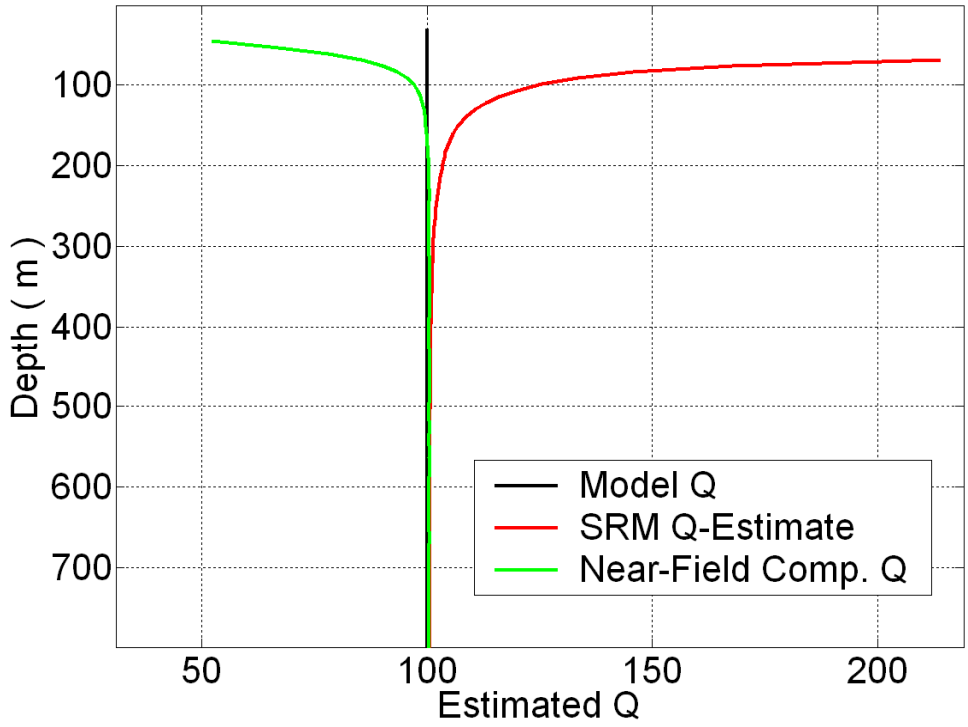

FIG. 17. Spectral ratio method Q-estimates with and without near-field compensation compared to the original model-Q of 100.